

# Machined phononic crystals to block high-order Lamb waves and crosstalk in through-metal ultrasonic communication systems

Cite as: Appl. Phys. Lett. **120**, 191705 (2022); doi: [10.1063/5.0083380](https://doi.org/10.1063/5.0083380)

Submitted: 24 December 2021 · Accepted: 19 April 2022 ·

Published Online: 12 May 2022





View Online



Export Citation



CrossMark

Christopher Sugino,<sup>1,a)</sup>  Romain Gerbe,<sup>2</sup> Ehren Baca,<sup>3</sup> Charles Reinke,<sup>3</sup> Massimo Ruzzene,<sup>2</sup> Alper Erturk,<sup>1</sup>  and Ihab El-kady<sup>3</sup>

## AFFILIATIONS

<sup>1</sup>George W. Woodruff School of Mechanical Engineering, Georgia Institute of Technology, Atlanta, Georgia 30332, USA

<sup>2</sup>Paul M. Rady Mechanical Engineering, University of Colorado Boulder, Boulder, Colorado 80309, USA

<sup>3</sup>Sandia National Laboratories, Albuquerque, New Mexico 87123, USA

**Note:** This paper is part of the APL Special Collection on Acoustic and Elastic Metamaterials and Metasurfaces.

<sup>a)</sup>Author to whom correspondence should be addressed: [csugino3@gatech.edu](mailto:csugino3@gatech.edu)

## ABSTRACT

For systems that require complete metallic enclosures (e.g., containment buildings for nuclear reactors), it is impossible to access interior sensors and equipment using standard electromagnetic techniques. A viable way to communicate and supply power through metallic barriers is the use of elastic waves and ultrasonic transducers, introducing several design challenges that must be addressed. Specifically, the use of multiple communication channels on the same enclosure introduces an additional mechanism for signal crosstalk between channels: guided waves propagating in the barrier between channels. This work numerically and experimentally investigates a machined phononic crystal to block MHz Lamb wave propagation between ultrasonic communication channels, greatly reducing wave propagation and the resulting crosstalk voltage. Blind grooves are machined into one or both sides of a metallic barrier to introduce a periodic unit cell, greatly altering the guided wave dispersion in the barrier. Numerical simulations are used to determine a set of groove geometries for testing, and experiments were performed to characterize the wave-blocking performance of each design. The best-performing design was tested using piezoelectric transducers bonded to the barrier, showing a 14.4 dB reduction in crosstalk voltage. The proposed periodic grooving method is a promising technique for completely isolating ultrasonic power/data transfer systems operating in a narrow frequency range.

Published under an exclusive license by AIP Publishing. <https://doi.org/10.1063/5.0083380>

There is a broad class of engineering applications in which wireless power or data transfer is required. For example, electronics operating in harsh environments, biomedical implants, or remote sensors may not be accessible using standard electrical cabling. In such situations, there are a variety of wireless power transfer (WPT) or contactless energy transfer (CET) techniques available, such as the commonly used inductive coupling.<sup>1</sup> However, for engineering systems that require complete metallic enclosures (e.g., containment buildings for nuclear reactors), standard electromagnetic techniques are made ineffective by the skin effect. A viable alternative way to communicate and supply power through metallic barriers is to use electromechanical transducers to send and receive ultrasonic waves. An electrical signal on one side of the barrier is provided as input to a transducer, generating an ultrasonic wave that propagates to the receiving transducer on the other side of the barrier. The receiver converts the ultrasonic wave

back into an electrical signal, creating an equivalent electrical transmission line that spans the metallic enclosure. This **ultrasonic communication** channel can be used to supply power via appropriate AC–DC conversion or to send/receive data using standard communication techniques. Many researchers have investigated and experimentally demonstrated this concept for individual channels on metal barriers,<sup>2–5</sup> and similar concepts have been explored for deeply implanted biomedical implants.<sup>6–10</sup>

Although there have been promising results for power and data transmission for a single communication channel on a metal barrier, it is desirable to have both power transmission and data transmission through multiple channels on a single barrier. These multichannel systems present a design challenge—specifically, the actuation of each transmitter generates guided waves that propagate in the barrier, potentially generating unwanted signal crosstalk on receivers

elsewhere on the barrier. This electromechanical crosstalk is especially important for data communication channels, which may have more stringent operating envelopes for effective data transmission and operate at a much lower voltage level than power transfer tiles. This problem was noted by Lawry *et al.*,<sup>11</sup> who investigated a system with simultaneous power and data transfer through a metal barrier. Their solution to the crosstalk problem was based purely on signal processing, adding filters to reduce the crosstalk voltage seen by the data transfer tiles and avoiding the crosstalk frequency and its harmonics using frequency-division multiplexing (FDM). The approach described here is intended to supplement these approaches—the complete mechanical isolation of power transfer tiles would potentially enable higher power throughput and reduced power requirements for data transfer. Additionally, the use of a mechanical filter for crosstalk would significantly enhance the robustness of the combined power and communication systems, which may be inaccessible after installation.

Thus, to further reduce crosstalk and expand the design space of multichannel mechanical communication systems, this work investigates a purely mechanical strategy for minimizing electromechanical signal crosstalk received by data transmission tiles. The approach takes inspiration from phononic crystal and metamaterial research,<sup>12–21</sup> introducing a periodic unit cell to alter the guided wave propagation characteristics in the barrier. Phononic crystals for Lamb waves have been explored by various researchers;<sup>22–26</sup> however, most of this research has been limited to relatively small frequency-thickness products ( $<4$  MHz mm), and many designs would introduce significant manufacturing challenges.

Here, a straightforward phononic crystal/metamaterial machining strategy is proposed to block the guided waves generated by power transfer tiles, controlling the propagating guided wave modes by periodically machining grooves into the barrier. Since the frequency-thickness product is 6.3 MHz mm for the considered system, high-order symmetric and antisymmetric Lamb waves (S0–S2 and A0–A2) can be excited in the barrier. As a result, there are multiple guided wave modes that can contribute to crosstalk, making it challenging to completely prevent wave propagation over a wide frequency range. However, for a power transfer tile operating over a narrow frequency range near resonance, groove designs can be optimized to block wave propagation at that specific frequency. Groove designs are obtained through numerical simulation and optimization, and a set of five designs are tested using an ultrasonic wedge transducer. The best-performing design is tested using piezoelectric transducers bonded to the barrier, demonstrating a 14.4 dB reduction in crosstalk voltage. This approach would allow power transfer tiles to be isolated fully from the rest of the metallic barrier, effectively eliminating the influence of their actuation on the ultrasonic communication channels on the barrier.

We consider a system of multiple mechanical communication channels, each comprising two opposing piezoelectric patches bonded on either side of a metallic barrier. The piezoelectric patches are poled through the thickness (normal to the barrier surface) for operation in the 33-mode. We assume that the opposing faces of each piezoelectric patch are covered by thin metallic electrodes, such that we can assume there is a constant voltage across each surface. By applying a voltage to one patch (i.e., the transmitter), elastic waves are generated that propagate to the opposite patch (i.e., the receiver), which generates an output voltage. At the same time, this actuation generates guided waves in the

barrier that can propagate to an adjacent communication channel, resulting in unwanted voltage measurements in the absence of direct actuation of that channel. The system is shown schematically in Fig. 1.

We aim to minimize crosstalk through the use of periodically machined grooves in the barrier, which are designed to minimize the guided wave propagation away from the tiles. This concept is inspired by the research in phononic crystals, which introduce a bandgap through a periodic array of a repeated unit cell.<sup>12</sup> These machined grooves must have geometry specifically tuned to the operating frequency of the power tiles, typically their fundamental resonant frequency, and they must maintain the desired electromagnetic shielding properties of the barrier (i.e., they cannot fully penetrate the barrier or reduce its thickness too significantly). We consider machining grooves on one or both sides of the barrier, as shown schematically in Figs. 1(b) and 1(c). The barrier has thickness  $h_b$ , and the grooves have width  $\Delta x$ , depth  $h$ , and unit cell size  $a$ . It should also be noted that this work only considers a subtractive manufacturing strategy in which material is removed from the barrier via machining. Similar additive manufacturing approaches could be considered in which waves are blocked by adding material to the barrier in a designed fashion. The additive approach may be necessary for very large structures that cannot be machined, but it introduces an additional interface between the barrier and the added material that must be modeled and optimized.

For concreteness, we consider a  $h_b = 3$  mm thick aluminum barrier. The actuated power transfer channel comprises two  $3\text{ cm} \times 3\text{ cm} \times 1\text{ mm}$  PZT-4 tiles (resonant frequency 2.1 MHz), and the adjacent crosstalk-receiving channel comprises a pair of  $1\text{ cm} \times 1\text{ cm} \times 0.4\text{ mm}$  tiles placed 2.5 cm from the actuated pair of tiles. To reduce computational effort, we assume that the grooves are machined parallel to one edge of the square tiles, and that the tile has lateral dimensions much greater than the relevant wavelengths in the barrier. Under these conditions, the assumptions of plane strain can be used to consider only a two-dimensional slice of the barrier perpendicular to the groove direction, since the guided waves generated by the tile will not vary significantly in the out-of-plane direction. For the purpose of this study, the groove width was kept at a minimum machinable value of  $\Delta x = 1$  mm, while the groove depth  $h$  and unit cell size  $a$  were varied to optimize the design. It should be noted that an ideal design would use a groove width on the order of the smallest wavelength propagating in the barrier; however, this is infeasible for high-order Lamb waves with submillimeter wavelengths as in the system here. Additionally, groove depth was constrained to the range  $0 < h \leq 0.6h_b$  to maintain a minimum thickness of 1.2 mm. Similarly, the unit cell size was constrained to  $1.5\text{ mm} \leq a \leq 2.5\text{ mm}$  for one-sided designs and  $3\text{ mm} \leq a \leq 5\text{ mm}$  for two-sided designs, maintaining a minimum spacing between grooves of 0.5 mm and ensuring that the overall footprint of the grooved region of the barrier was less than 2.5 cm. Other applications may require more sophisticated constraints that could be introduced to the optimization procedure; for example, pressure vessels may have a minimum required static stiffness that must be maintained after machining grooves.

A total of ten grooves were placed between the two communication channels, corresponding to 10 one-sided unit cells or five two-sided unit cells. Transient simulations were performed using a seven-cycle 2.1 MHz Gaussian sine burst as voltage input to one of the power transfer tiles. The transient simulation results are summarized using the root mean square (RMS) of the input voltage, direct output

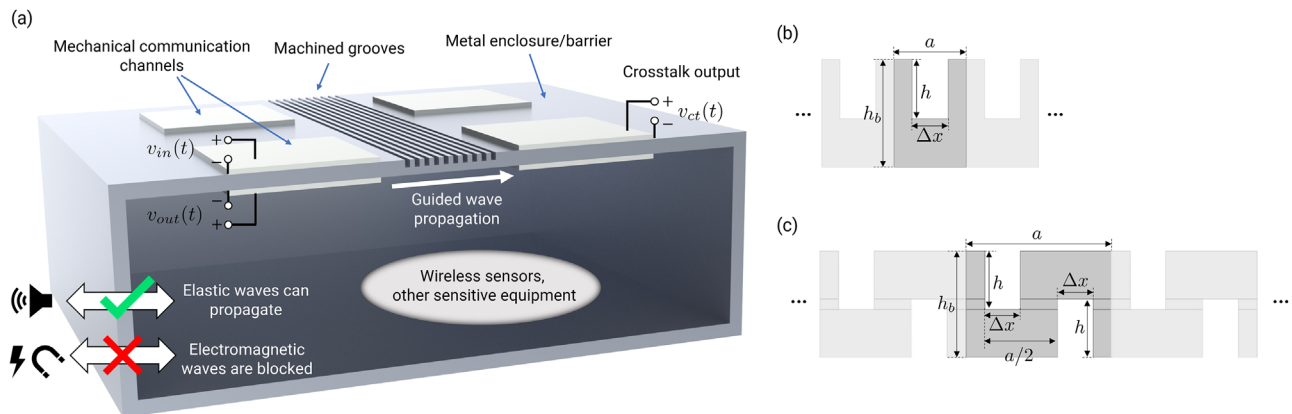


**FIG. 1.** (a) Schematic of the ultrasonic communication system. Actuating the left channel generates guided waves that propagate in the barrier to the right channel, resulting in a small crosstalk voltage  $v_{ct}$ . Grooves are machined into the barrier to reduce crosstalk. (b) Side view of the unit cell with one-sided grooving. (c) Side view of the unit cell with two-sided grooving.

voltage, and crosstalk voltage after a fixed simulation time of  $30 \mu\text{s}$  to give enough time for waves to propagate from the transmitting piezos to the adjacent communication channel. Parameter sweeps of the groove depth  $h$  and unit cell size  $a$  were performed to find the groove geometries with the best crosstalk reduction performance, with results shown in Fig. 2.

Considering the results of Figs. 2(a) and 2(b), it is clear that both one-sided and two-sided grooving are effective at reducing crosstalk, with a maximum reduction in RMS crosstalk voltage of 86.8% (17.6 dB) and 91.2% (21.1 dB) for one- and two-sided grooving, respectively. One-sided designs are significantly simpler to manufacture, requiring machining only on one side of the barrier. Still, there is some benefit to two-sided machining: Fig. 2(a) shows that excellent crosstalk reduction can be achieved with the two-sided design over a wide range of parameter values (i.e.,  $h/h_b > 0.5$  and  $a > 3.7 \text{ mm}$ ), reducing the effects of slight machining variation between subsequent grooves.

The parametric sweep results of Fig. 2 show that periodically machining grooves into the barrier are an effective strategy for reducing crosstalk. To develop further intuition into the mechanism of crosstalk reduction, we next consider the dispersion characteristics of selected groove geometries. The dispersion curves describe which guided wave modes are able to propagate through the machined section of the barrier. To obtain the dispersion curves, we consider 2D plane strain finite element models of a single unit cell with Floquet periodic boundary conditions along the propagation direction with wavenumber  $k$ . The dispersion diagrams of the best-performing designs of Figs. 2(a) and 2(b) are shown in Fig. 3.

The dispersion results show that the best-performing groove geometries both exhibit a bandgap near to or including the operating frequency of the actuated tiles. The one-sided design [Fig. 3(a)] has a bandgap from 2.1 to 2.13 MHz, whereas the two-sided design [Fig. 3(b)] has a bandgap from 2.07 to 2.17 MHz. The wave modes at the edges in each bandgap (inset in Fig. 3) help explain the crosstalk performance of each design. For the one-sided design, there are only two wave modes near the operating frequency of 2.1 MHz. Additionally, the wave mode at 2.1 MHz exhibits motion that is dominantly

localized on the bottom surface of the barrier, producing minimal crosstalk on the top surface of the barrier at the receiving tile. Additionally, the stub that is formed between two adjacent grooves exhibits some resonant behavior: at frequencies above the bandgap,

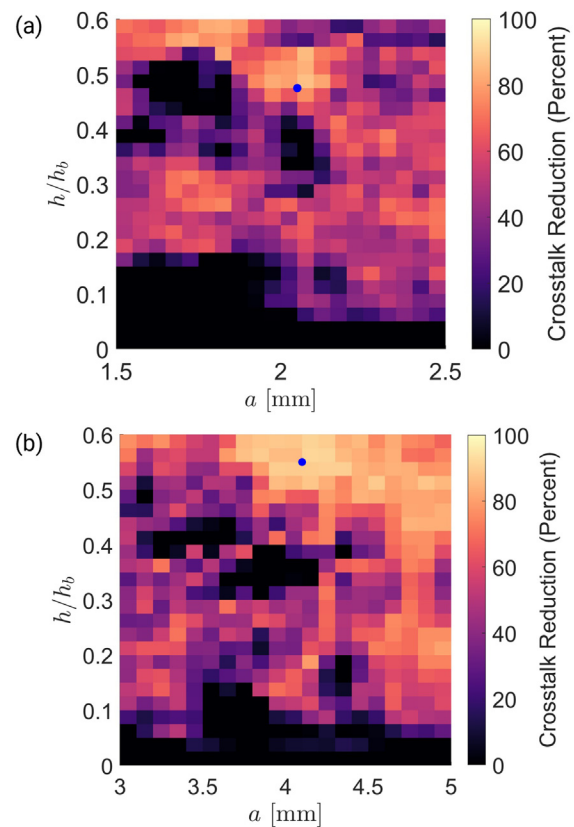


**FIG. 2.** Crosstalk reduction as a function of normalized groove depth  $h/h_b$  and unit cell size  $a$  for a fixed groove width  $\Delta x = 1 \text{ mm}$  for (a) one-sided grooving and (b) two-sided grooving. The blue points indicate the best-performing design for each study.

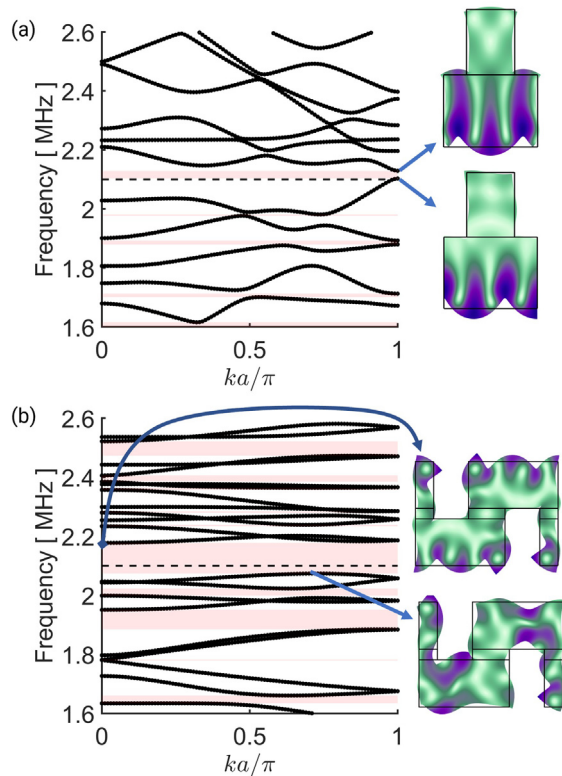


**FIG. 3.** Dispersion diagrams and selected mode shapes for the best-performing designs from Fig. 2 for (a) one-sided grooving ( $h/h_b = 0.475$ ,  $a = 2.05$  mm) and (b) two-sided grooving ( $h/h_b = 0.55$ ,  $a = 4.1$  mm). The dashed line indicates the center frequency of excitation for the transient studies, and the shaded regions indicate bandgaps.

the stub motion is symmetric about the normal axis of the barrier, while below the bandgap, the motion is asymmetric. These two stub motions couple to the barrier in different ways—the lower-frequency mode couples to a surface wave on the bottom surface, whereas the higher-frequency mode couples to a wave that has motion through the entire thickness. Because these two distinct stub and wave motions exist at close frequencies to each other, they are able to mix and form a narrow bandgap. Two-sided grooving introduces even more significant mode mixing, as shown by the wave modes at the edges of the bandgap in Fig. 3(b). In this case, wave propagation through the coiled pathway formed between adjacent grooves creates significantly more complex barrier motion. As shown by the inset of Fig. 3(b), at frequencies above the bandgap, motion is largely localized to the un-machined surface of the barrier. At frequencies below the bandgap, the wave motion is more evenly distributed through the cross section of the barrier. Again, the close frequency proximity of these two wave motions enables significant mode mixing and the formation of a relatively wideband gap. It is notable that in both the one-sided and two-sided cases, the bandgap forms between a surface wave mode and a through-thickness wave mode.

It should be noted that the calculated designs can potentially be applied to other barrier thicknesses or crosstalk frequencies. Each dispersion curve specifies a relationship between dimensionless frequency

$\omega h_b/c_s$  and wavenumber  $ka/\pi$ , where  $\omega$  is the frequency and  $c_s$  is the material shear wave velocity. As a result, scaling the entire geometry of the unit cell inversely scales the frequency and wavenumber of a given wave mode. For example, scaled versions of the groove designs in Fig. 3 could be used in a barrier that is twice as thick by reducing the targeted frequency by a factor of two. However, constraints on frequency, thickness of the barrier, and/or the smallest machinable feature size may necessitate the optimization of additional designs (e.g., for thick barriers at relatively high frequencies). In the future, it would be beneficial to develop a library of groove designs that operate in different frequency and thickness regimes.

For experimental validation of the proposed grooving strategy, we selected a set of five locally optimal designs from the results of Fig. 2 to fabricate and test, as summarized in Table I. A set of 3 mm thick aluminum barriers were machined using a 1 mm end mill according to the groove geometries in Table I. For the one-sided designs, a total of 21 grooves were milled (i.e., 21 unit cells), and for the two-sided designs, a total of 22 grooves were milled (i.e., 11 unit cells). First, each groove design was tested using a scanning laser Doppler vibrometer (SLDV), which measures the out-of-plane velocity wavefield across the surface of the barrier. An ultrasonic wedge transducer (Olympus C546-SM, center frequency 3.5 MHz) was used to excite Lamb waves at a center frequency of 2.1 MHz and the SLDV measured surface velocity at a sample rate of 12.5 MHz. This experiment was designed to measure the wave-blocking capabilities of each groove design, and hence, wave propagation was measured along lines perpendicular to the grooves. The experimental setup is shown in Fig. 4(a), and a summary of the performance of each groove design is shown in Fig. 4(b). All five designs reduced the RMS wave velocity across the grooved section of the barrier. Design G2.2 was the best-performing design in terms of wave attenuation, reducing the RMS wave velocity by 87% (17.7 dB) from one side of the grooved region to the other. Note that all the designs performed worse in experiments than in the numerical simulations, which may be due to sensitivity of the designs to the material properties of aluminum or the variation between the machined barrier and the exact, perfectly periodic unit cell from simulations. For example, the numerical simulations show that design G2.2 is not very sensitive to geometry, located in the upper-right quadrant of Fig. 2(b). By contrast, small variations in geometry for the other designs may significantly reduce the crosstalk-reduction performance.

To characterize the crosstalk-reduction capability of the periodic grooves, design G2.2 (the best-performing design) was tested using more realistic piezoelectric transducers bonded to the barrier.

**TABLE I.** Summary of the tested groove geometries and their numerically predicted performance.

Label	Sides	Groove depth ( $h$ ) (mm)	Unit cell size ( $a$ ) (mm)	Crosstalk reduction (dB)
G1.1	One	1.43	2.05	17.7
G1.2	One	0.75	1.80	11.8
G2.1	Two	1.65	4.10	21.5
G2.2	Two	1.50	4.50	19.2
G2.3	Two	0.53	4.10	13.7



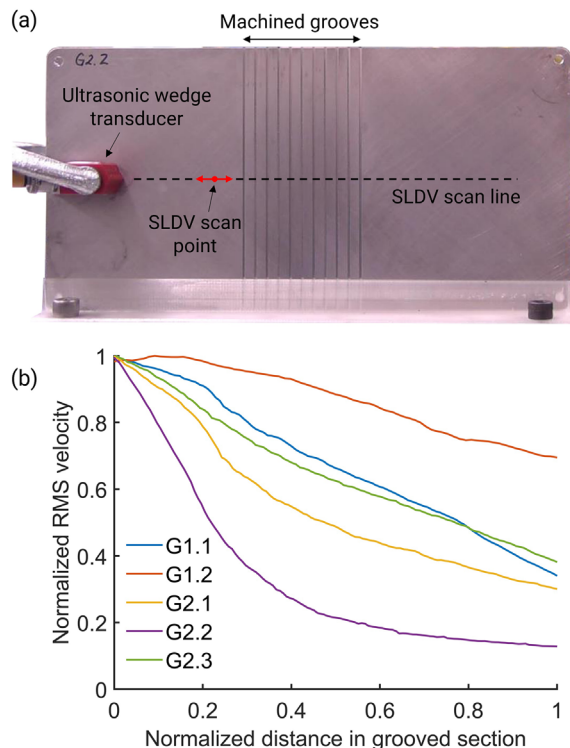


**FIG. 4.** (a) Experimental setup. An ultrasonic wedge transducer excites guided waves that are measured using a scanning laser Doppler vibrometer (SLDV), which measures the out-of-plane velocity along the shown scan line. (b) RMS velocity vs distance along the grooved section for the groove designs of Table I. For each design, performance is averaged over three positions along the grooves.

The experimental setup is shown in Fig. 5(a). A single  $3\text{ cm} \times 3\text{ cm} \times 1\text{ mm}$  PZT-4 tile was bonded near the grooved section of the barrier to emulate a power transfer tile, while two  $1\text{ cm} \times 1\text{ cm} \times 0.5\text{ mm}$  PZT-4 tiles were bonded on either side of the larger tile to emulate crosstalk-receiving data transfer tiles. In this way, one of the data transfer tiles (tile A in Fig. 5) is not protected by the periodic grooves, whereas the other (tile B in Fig. 5) is protected by grooves. For this experiment, a seven-cycle Gaussian sine burst at 2.1 MHz was used as voltage input to the power transfer tile, while the SLDV was used to measure the RMS surface velocity over the relevant section of the barrier. Additionally, the voltage on each data transfer tile was recorded to compare the received crosstalk voltage. The RMS surface velocity is shown in Fig. 5(a), and the crosstalk voltages on the two data tiles are shown in Fig. 5(b).

It is clear from Fig. 5(a) that the surface velocity of the barrier is greatly reduced by the grooves, such that the velocity near tile B is significantly smaller than the velocity close to tile A. This is also reflected on the voltage seen by each tile in Fig. 5(b), which highlights that tile B had significantly reduced crosstalk voltage (14.4 dB reduced RMS) compared to tile A. Overall, this validates the use of grooves to minimize crosstalk, simplifying the design process ultrasonic communication systems with simultaneous power and data transfer. For example, power transfer transducers could be paired with an appropriate groove geometry, enabling the placement of isolated power transfer channels

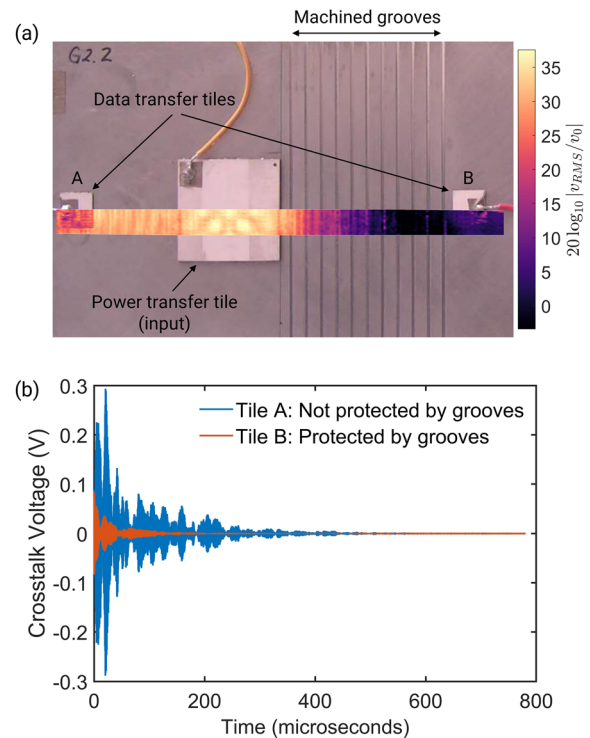


**FIG. 5.** (a) Image of the experimental setup for groove design G2.2 with bonded piezoelectric transducers. The measured RMS surface velocity in response to a seven-cycle 2.1 MHz Gaussian sine burst voltage excitation is overlaid on the image. (b) Comparison of the measured crosstalk voltage on the two data transfer tiles shown in (a). Time histories are shown with a  $20\text{ }\mu\text{s}$  delay to give sufficient time for guided wave propagation and neglect transient capacitive coupling between the tiles.

that would not affect the design or performance of communication channels elsewhere on the barrier.

In conclusion, this work has investigated the use of periodically machined grooves to minimize guided wave propagation between ultrasonic communication channels on a metallic barrier. The groove geometry can be tuned to the operating frequency of the power transfer channels, preventing or greatly reducing guided wave propagation away from the tiles by creating a guided wave bandgap in the machined section of the barrier. Several groove designs were obtained through numerical optimization and finite element modeling, and each design was tested using an ultrasonic wedge transducer and scanning laser Doppler vibrometer to validate their Lamb wave-blocking performance. The best performing design (G2.2) reduced the RMS surface velocity by 87% over a distance of 10 cm. This design was then tested using piezoelectric transducers, resulting in a 14.4 dB reduction in crosstalk voltage. This strategy of grooving to isolate tiles would be easily extended to 2D, allowing power transfer tiles to be fully surrounded by grooves and isolated from the rest of the barrier. Such isolation would free the design process for barriers with multiple ultrasonic communication channels, potentially expanding the usable frequency range for data transfer. On the other hand, machining grooves into existing barriers may be impractical; instead, individual

panels that are machined and instrumented with ultrasonic transducers could be incorporated with larger structures.

Sandia National Laboratories is a multimission laboratory managed and operated by National Technology & Engineering Solutions of Sandia, LLC, a wholly owned subsidiary of Honeywell International Inc., for the U.S. Department of Energy's National Nuclear Security Administration under Contract No. DE-NA0003525. This paper describes objective technical results and analysis. Any subjective views or opinions that might be expressed in the paper do not necessarily represent the views of the U.S. Department of Energy or the United States Government, SAND2022-5838 J.

## AUTHOR DECLARATIONS

### Conflict of Interest

The authors have no conflicts to disclose.

### DATA AVAILABILITY

The data that support the findings of this study are available from the corresponding author upon reasonable request.

## REFERENCES

- <sup>1</sup>G. A. Covic and J. T. Boys, "Inductive power transfer," *Proc. IEEE* **101**, 1276–1289 (2013).
- <sup>2</sup>Y. Hu, X. Zhang, J. Yang, and Q. Jiang, "Transmitting electric energy through a metal wall by acoustic waves using piezoelectric transducers," *IEEE Trans. Ultrason. Ferroelectr. Freq. Control* **50**, 773–781 (2003).
- <sup>3</sup>H. Hu, Y. Hu, C. Chen, and J. Wang, "A system of two piezoelectric transducers and a storage circuit for wireless energy transmission through a thin metal wall," *IEEE Trans. Ultrason. Ferroelectr. Freq. Control* **55**, 2312–2319 (2008).
- <sup>4</sup>M. Kluge, T. Becker, J. Schalk, and T. Otterpohl, "Remote acoustic powering and data transmission for sensors inside of conductive envelopes," in *Sensors, 2008 IEEE* (IEEE, 2008), pp. 41–44.
- <sup>5</sup>D. J. Graham, J. A. Neasham, and B. S. Sharif, "Investigation of methods for data communication and power delivery through metals," *IEEE Trans. Ind. Electron.* **58**, 4972–4980 (2011).
- <sup>6</sup>A. Denisov and E. Yeatman, "Ultrasonic vs. inductive power delivery for miniature biomedical implants," in *2010 International Conference on Body Sensor Networks* (IEEE, 2010), pp. 84–89.
- <sup>7</sup>J. Charthad, M. J. Weber, T. C. Chang, and A. Arbabian, "A mm-sized implantable medical device (IMD) with ultrasonic power transfer and a hybrid bi-directional data link," *IEEE J. Solid-State Circuits* **50**, 1741–1753 (2015).
- <sup>8</sup>H. Basaeri, D. B. Christensen, and S. Roundy, "A review of acoustic power transfer for bio-medical implants," *Smart Mater. Struct.* **25**, 123001 (2016).
- <sup>9</sup>H. Basaeri, Y. Yu, D. Young, and S. Roundy, "A MEMS-scale ultrasonic power receiver for biomedical implants," *IEEE Sens. Lett.* **3**, 1–4 (2019).
- <sup>10</sup>R. Hinchet, H.-J. Yoon, H. Ryu, M.-K. Kim, E.-K. Choi, D.-S. Kim, and S.-W. Kim, "Transcutaneous ultrasound energy harvesting using capacitive triboelectric technology," *Science* **365**, 491–494 (2019).
- <sup>11</sup>T. J. Lawry, K. R. Wilt, J. D. Ashdown, H. A. Scarton, and G. J. Saulnier, "A high-performance ultrasonic system for the simultaneous transmission of data and power through solid metal barriers," *IEEE Trans. Ultrason. Ferroelectr. Freq. Control* **60**, 194–203 (2012).
- <sup>12</sup>M. S. Kushwaha, P. Halevi, L. Dobrzynski, and B. Djafari-Rouhani, "Acoustic band structure of periodic elastic composites," *Phys. Rev. Lett.* **71**, 2022 (1993).
- <sup>13</sup>J. Li and C. T. Chan, "Double-negative acoustic metamaterial," *Phys. Rev. E* **70**, 055602 (2004).
- <sup>14</sup>S. A. Cummer, B.-I. Popa, D. Schurig, D. R. Smith, J. Pendry, M. Rahm, and A. Starr, "Scattering theory derivation of a 3D acoustic cloaking shell," *Phys. Rev. Lett.* **100**, 024301 (2008).
- <sup>15</sup>A. N. Norris and A. L. Shuvalov, "Elastic cloaking theory," *Wave Motion* **48**, 525–538 (2011).
- <sup>16</sup>H. Zhu and F. Semperlotti, "Metamaterial based embedded acoustic filters for structural applications," *AIP Adv.* **3**, 092121 (2013).
- <sup>17</sup>B.-I. Popa and S. A. Cummer, "Non-reciprocal and highly nonlinear active acoustic metamaterials," *Nat. Commun.* **5**, 3398 (2014).
- <sup>18</sup>H. Zhu and F. Semperlotti, "Phononic thin plates with embedded acoustic black holes," *Phys. Rev. B* **91**, 104304 (2015).
- <sup>19</sup>S. A. Cummer, J. Christensen, and A. Alù, "Controlling sound with acoustic metamaterials," *Nat. Rev. Mater.* **1**, 16001 (2016).
- <sup>20</sup>S. Babaei, J. T. Overvelde, E. R. Chen, V. Tournat, and K. Bertoldi, "Reconfigurable origami-inspired acoustic waveguides," *Sci. Adv.* **2**, e1601019 (2016).
- <sup>21</sup>O. R. Bilal, A. Foehr, and C. Daraio, "Reprogrammable phononic metasurfaces," *Adv. Mater.* **29**, 1700628 (2017).
- <sup>22</sup>J. Gao, X.-Y. Zou, J.-C. Cheng, and B. Li, "Band gaps of lower-order Lamb wave in thin plate with one-dimensional phononic crystal layer: Effect of substrate," *Appl. Phys. Lett.* **92**, 023510 (2008).
- <sup>23</sup>Y. Cheng, X. Liu, and D. Wu, "Band structure of a phononic crystal plate in the form of a staggered-layer structure," *J. Appl. Phys.* **109**, 064904 (2011).
- <sup>24</sup>H.-B. Zhang, J.-J. Chen, and X. Han, "Lamb wave band gaps in a homogenous plate with periodic tapered surface," *J. Appl. Phys.* **112**, 054503 (2012).
- <sup>25</sup>P. Wang, T.-N. Chen, K.-P. Yu, and X.-P. Wang, "Lamb wave band gaps in a double-sided phononic plate," *J. Appl. Phys.* **113**, 053509 (2013).
- <sup>26</sup>Y.-F. Wang, T.-T. Wang, J.-P. Liu, Y.-S. Wang, and V. Laude, "Guiding and splitting Lamb waves in coupled-resonator elastic waveguides," *Compos. Struct.* **206**, 588–593 (2018).